AIAA 89-1850
Inception Length to a Fully-Developed Fin-Generated Shock Wave Boundary-Layer Interaction

F. Lu
University of Texas
Arlington, TX
G. Settles
Pennsylvania State Univ.
University Park, PA

AIAA 20th Fluid Dynamics, Plasma Dynamics and Lasers Conference
Buffalo, New York / June 12–14, 1989

AIAA-89-1850

Inception Length to a Fully-Developed Fin-Generated Shock Wave Boundary-Layer Interaction

Frank K. Lu*
The University of Texas at Arlington, Arlington, Texas
and
Gary S. Settles†
The Pennsylvania State University, University Park, Pennsylvania

An experimental study of fin-generated shock wave turbulent boundary-layer interactions confirmed previous observations that, sufficiently far from the fin apex, such interactions become conical. The inception length to conical symmetry was found to increase weakly with Mach number for Mach numbers from 2.5 to 4 and fin angles from 4° to 22°. For the range of interactions examined, the inception length was found to depend primarily upon the inviscid shock angle, this angle ranging from 21° to 40°. The behavior of the inception length with shock angle can be broadly divided into two categories. For "weak" interactions with shock angles less than about 35°, the inception length decreased as the shock angle increased. For "strong" interactions with shock angles greater than about 35°, the inception region was small and was approximately constant at three boundary-layer thicknesses in length. In the latter, strong interaction case, the inception length was an order of magnitude smaller than that found in the weakest interactions examined, to the extent that strong interactions were practically fully-developed from the apex.

Nomenclature

M_n = $M_\infty \sin\beta_o$, Mach number normal to the inviscid shock-wave trace on the test surface
M_∞ = incoming freestream Mach number
s, θ = polar coordinate system centered at fin apex (Fig. 2b)
Re_δ = Reynolds number based on the undisturbed boundary-layer thickness at the start of the interaction
α = angle made by fin with respect to the incoming freestream direction
β = angle made by surface-flow features with respect to the incoming freestream direction
δ = undisturbed boundary-layer thickness at the start of the interaction
ξ, η, ζ = orthonormal coordinate system based on the inviscid shock-wave trace on the test surface (Fig. 2b)

Superscripts
$(\bar{})$ = normalized by δ

Subscripts
i = inception
U = upstream influence
∞ = incoming freestream conditions

1 Introduction

An important class of fluid dynamics problems is that of shock wave boundary-layer interactions. These interactions are important because of their ubiquitous presence in high-speed flight. Recently, their understanding has taken on further importance arising from the development of hypersonic flight vehicles such as the National Aerospace Plane. For example, the complicated shock boundary-layer interactions in engine inlets need to be accurately predicted for the engine's performance to be determined. However, present predictions are generally poor, especially if the boundary layer is separated. It is precisely this separated interaction, with its attendant problems (e.g., flow unsteadiness, high heat-transfer rates and massive distortions of the main flow) which is of concern and which is spurring present research into shock boundary-layer interactions.

*Asst. Prof., Aerospace Eng. Dept., Member AIAA.
†Prof. & Dir., Gas Dynamics Lab., Mech. Eng. Dept., Assoc. Fellow AIAA.

Shock wave boundary-layer interactions are conveniently divided into two-dimensional (2D) and three-dimensional (3D) types. 2D interactions are nominally normal to the streamwise direction while 3D interactions possess greater geometrical variety. A recent review has succinctly classified 3D interactions into two broad classes: dimensional and dimensionless types [1]. Dimensional types have explicit geometrical length scales such as a diameter or a thickness while dimensionless types, obviously, have no length scales except those due to the flow itself (such as δ).

One configuration that produces a dimensionless interaction is a fin mounted on a flat plate. The fin generates a shock sweeping across an incoming turbulent boundary layer (Fig. 1). This idealized configuration represents practically-occurring situations such as at fin-fuselage junctions or in supersonic engine inlets. A review of such fin-generated shock wave turbulent boundary-layer interactions can be found in Ref. [2]. Thus, the following review will be narrowed to the inception-length issue under examination.

In studying shock wave boundary-layer interactions, the so-called mean surface "footprint" is revealed by surface-flow visualization [3, 4]. An example of a surface-flow pattern of an interaction is shown in Fig. 2(a) while the pattern's key features are identified in Fig. 2(b). The fin is placed at an angle α to the incoming stream which generates an inviscid shock wave impinging the test surface at an angle β_o. In a viscous flow, the shock wave represents an adverse pressure gradient which the boundary layer must overcome. The interaction between two essentially disparate flow phenomena, the shock wave and the boundary layer, starts at the upstream-influence line (or, the interaction onset). In surface-flow visualization, this is detected by the onset of deflection of the incoming surface streaks. Separation occurs if the shock is strong enough and is marked by a severe turning of the surface flow, resulting in a convergence of the surface streaks. From topological rules, an attachment line is associated with the separation line [5]. There is ample evidence that an "open" separation with a strong, swept vortical flow exists in such cases [6, 7]. It is also thought that a supersonic turbulent jet impinges the test surface at the attachment line, resulting in overpressures and high heat transfer at this region [6]. For the strongest interactions, a secondary separation is also observed (computationally as well [8]) although not much is known about this phenomenon.

The surface-flow pattern in a 3D shock-wave boundary-layer interaction shows an "inception region" near the fin leading edge and a farfield region further away, Fig. 2(b) [9]. Familiar examples of such nearfield and farfield behavior include pipe inlet flows, wakes and jets. For fin-generated interactions, the surface features ahead of the inviscid shock in the farfield appear to radiate from a virtual origin, exhibiting "conical symmetry" (Fig. 2) [10], while for the region between the inviscid shock and the fin, conical symmetry is approximately valid. Cylindrical symmetry, one the other hand, occurs where the farfield interaction is parallel to the inviscid shock and can be found in certain other interactions such as those generated by some swept compression corners or swept steps [1]. This issue of conical and cylindrical symmetry has raised some controversy, especially for fin interactions [11, 12]. Inger [13] showed analytically, however, that the conical nature of the inviscid flowfield dominates the interaction, forcing the interaction to eventually take on an asymptotically conical form even though the boundary-layer growth is nonconical.

The surface features of conical interactions can be appropriately quantified by a polar coordinate system, (r, β), centered at the virtual origin as illustrated in Fig. 2(b). In addition to the polar coordinate system, a Cartesian coordinate system, (ξ, ζ), centered on the fin apex may be used. The (ξ, ζ) coordinate system is an excellent approximation to the (r, β) polar coordinate system because the opening angle between the upstream-influence asymptote and the freestream shock angle, $(\beta_U - \beta_o)$, is small, typically less than 15°.

A detailed examination of the (conical) farfield interaction showed that a reduced upstream-influence angle, $\Delta\beta_U = (\beta_U - \mu_\infty)$, scales with a reduced shock angle, $\Delta\beta_o = (\beta_o - \mu_\infty)$, for $2.5 \leq M_\infty \leq 4$ and $0 \leq \Delta\beta_o \leq 20°$, where μ_∞ is the Mach angle of the incoming freestream [14]. Obviously, for conical symmetry, $\Delta\beta_U > \Delta\beta_o$ and for cylindrical symmetry, $\Delta\beta_U = \Delta\beta_o$. Lu *et al.* [14] fitted their data as

$$\Delta\beta_U = 2.2\Delta\beta_o - 0.027\Delta\beta_o^2. \qquad (1)$$

For small $\Delta\beta_o$, data scatter may give the impression of cylindrical symmetry. Such was the case for many previous studies where $\Delta\beta_o < 5°$. The poor resolution of the upstream-influence line for such weak interactions has also compounded the difficulty in its location. In addition, many measurements, due to facility limitations, were performed inside the inception zone. These problems added to the confusion over whether the interaction is conical or cylindrical, since most previous swept interaction studies were not meant to address this issue specifically. Lu *et al.* [14] also postulated that, at the large $\Delta\beta_o$ limit, $\Delta\beta_U \rightarrow \Delta\beta_o$, i.e., there would be cylindrical symmetry in this limiting situation. Experimental limitations, however, have thus far prevented observation of this behavior.

In a series of studies [10, 15, 16], the spanwise development of the upstream influence was found to scale according to

$$\tilde{\zeta}_U/M_n = f(\tilde{\xi}_U), \qquad (2)$$

where

$$\tilde{\xi}_U = (\xi_U/\delta)\, Re_\delta^b, \quad \tilde{\zeta}_U = (\zeta_U/\delta)\, Re_\delta^a, \qquad (3)$$

and $M_n = M_\infty \sin\beta_o$, (ξ_U, ζ_U) being the coordinates of the upstream-influence line. Eq. (2) was validated for Mach 3 interactions where $a = b = 1/3$ are empirical constants. The cited references identified the effect of the viscous parameters, δ and Re_δ, and the inviscid shock-strength parameter, M_n, on the upstream influence. Eq. (2) also shows that M_n and the (ξ, ζ) coordinate system accounts for α effectively. However, the upstream-influence scaling results at Mach 3 have not been extended to other Mach numbers to fully account for the effects of M_∞. A subsequent paper will examine this issue.

The departure from the farfield asymptote to the upstream-influence line is usually considered to be the inception point. At $M_\infty = 3$, Settles [17] found that

$$\tilde{\xi}_i \approx 1130 \cot\beta_o, \tag{4}$$

$\tilde{\xi}_i = (\xi_i/\delta)Re_\delta^b$ being the nondimensional inception length according to Eq. (3). Essentially, Eq. (4) shows that experiments tailored to examine the farfield should be performed outside the nondimensional inception region. Inger [13] examined the problem analytically and found that

$$\xi_i = C\zeta_i \cot\beta_o, \tag{5}$$

where C is a constant of order unity. Further, Eq. (2) implies a constant nondimensional value of $\tilde{\xi}_i$ which was given in Ref. [10] as

$$\tilde{\xi}_i \approx 1600. \tag{6}$$

The different inception-length scaling constants proposed in Eqs. (4) and (6) reflect the fact that the inception zone and the farfield merge gradually so that the inception length may not be specified with high precision.

To broaden our understanding of fin-generated interactions, a study was recently completed [2] covering a Mach number range from 2.5 through 4. This paper presents results from the database of Ref. [2] pertaining to the inception length, especially regarding its change with shock strength and Mach number.

2 Experimental Methods

2.1 Wind Tunnel and Test Models

The experiments were done in the Gas Dynamics Laboratory of the Pennsylvania State University. The Supersonic Wind Tunnel test facility is a blowdown wind tunnel with a test Mach number of 1.5 through 4, varied by an asymmetric sliding-block nozzle. The test section is 150 mm (6 in) wide, 165 mm (6.5 in) high and 610 mm (24 in) long. Further description of the wind tunnel and the experiments can be found in Ref. [2].

A flat plate, 500 mm (19.5 in) long, spanning the tunnel and mounted in the test section, provided the interaction test surface. On this plate was mounted a sharp-edged fin that generated a swept shock across the boundary layer that developed on the plate. The fin had a 10°-sharp leading edge and was placed with its tip 216 mm (8.5 in) from the plate leading edge and 26.2 mm (1.03 in) from the tunnel sidewall. The fin was 100 mm (4 in) high, 127 mm (5 in) long and 10.3 mm (0.404 in) thick. The fin height of about 30δ was therefore sufficient to ensure that the interaction was a semi-infinite one [18]. The length of the fin was chosen to provide the maximum interaction extent while allowing sufficiently large α to be obtained without stalling the wind tunnel.

The fin was held tightly onto the flat plate by a pneumatically-driven rotation mechanism mounted on the tunnel sidewall. A rubber seal at the bottom of the fin ensured that no leakage under the fin occurred during the tests. The fin-rotation mechanism rotated the fin to a predetermined α once test conditions were established. This was necessary only for tests with α larger than approximately 14°; at lower angles, α was fixed before the run. In the experiments, α ranged from 4° to 22°, the largest value being limited by tunnel stall. The fin angle was determined to 0.1° accuracy using a machinist's protractor.

2.2 Test Conditions

The experiments were performed at $M_\infty = 2.47$, 2.95, 3.44 and 3.95 (Table 1). Since the wind tunnel is a blowdown type, the stagnation temperature, T_o, decreased somewhat during a run. Typically, for a run of about 20 s, T_o dropped from 300 K (540°R) to 290 K (520°R). The nominal freestream unit Reynolds number, Re, was held relatively constant throughout the Mach number range at 50 to 80 $\times 10^6$ m^{-1} (15 to 24 $\times 10^6$/ft).

For each run, the Mach numbers were computed from the stilling chamber (stagnation) pressure, p_o, and a static pressure, p, measured from an orifice on the test surface ahead of the interaction, and assuming perfect-gas behavior. The unit Reynolds number, Re, was computed using p_o, T_o, p and the viscosity-temperature relation of Ref. [19]. The values of the test conditions and their standard deviations shown in Table 1 are not of "typical" runs but were obtained from the ensemble of runs of each Mach number throughout the test program. This is felt to provide a better characterization of the tests which were performed over an extended period.

Fig. 3 shows the undisturbed centerline boundary-layer velocity profiles, subjected to the van Driest II transformation, in law-of-the-wall coordinates. (No surveys at $M_\infty = 3.95$ were available during this study.) The figures also show the Sun-Childs [19] wall-wake curvefits to the data. Detailed surveys along the flat-plate centerline and 38 mm (1.5 in) to each side showed that the boundary layers were two-dimensional. Based

on these surveys, the boundary layers were considered to be turbulent and in equilibrium at the test region. In addition, the boundary layers were approximately adiabatic. Some centerline boundary-layer parameters based on the wall-wake curvefits at 216 mm (8.5 in) from the flat-plate leading edge are listed in Table 2. Data at $M_\infty = 3.95$ were obtained by linear extrapolation of lower Mach-number data.

2.3 Experimental Techniques

Temperature and pressure data were digitized and stored in a microcomputer. The computer was used to display tunnel conditions during a test and to analyze data. Further data analysis was performed on a mainframe computer.

The surface-flow features were visualized using a kerosene-pigment dry-transfer technique [3, 4]. Spatial data obtained from full-size undistorted images of the surface pattern (preserved on matte acetate tape) were, on average, resolved to 0.5 mm (0.02 in.). These data were digitized manually using a digitizing pad and stored in a microcomputer for analysis. Angular data were accurate to $\pm 0.5°$ for stronger interactions, but accuracy can be as poor as $\pm 3°$ for weak interactions due to difficulty in discerning weak surface-flow features.

2.4 Data Analysis

All of the digitized upstream-influence lines are plotted in Fig. 4(a) through Fig. 4(d). Fig. 5 is an example of the upstream-influence line in order to illustrate the data analysis described below. Closer examination of the figure shows a slight bulge to the upstream-influence line within the inception region. (Notice also the bulge in the separation line in Fig. 2(a).) This feature is particularly obvious in separated interactions and was first observed by Stalker [20] in swept step interactions. There are no explanations as yet on this phenomenon.

The inception point was determined by the following procedure. A straight-line asymptote was fitted to the farfield portion of the upstream-influence line. (This also allowed β_U to be determined [14].) The departure of this straight line from the actual upstream influence was taken to be the inception point, $I(x_i, z_i)$, as can be seen in Fig. 5. The figure also shows the virtual origin, V, as the intersection of the upstream-influence asymptote and the inviscid shock-wave trace. In practice, the upstream-influence data were replaced by a fourth-order curvefit that smoothed out the data scatter. Furthermore, the farfield upstream influence was replaced by the straight-line asymptote. The criterion for locating I was made objective by setting the fractional departure of the z-coordinate from this straight line to be equal to a small number, c_i, i.e.,

$$|z_i - z_{i_{asym}}|/z_i = c_i. \qquad (7)$$

With $c_i = 0.0001$, estimates of (x_i, z_i) were not substantially different from the visual estimates in Ref. [2]. Either visually or with Eq. (7), $I(x_i, z_i)$ was difficult to locate for weaker interactions, thereby resulting in larger errors. An error estimate was also performed, where the error bars of (x_i, z_i) for each test case were given by the 95% confidence levels to the upstream-influence data of Fig. 4. Finally, in the shock-based coordinate system,

$$\begin{aligned} \xi_i &= x_i \cos\beta_o + z_i \sin\beta_o \\ \zeta_i &= -x_i \sin\beta_o + z_i \cos\beta_o. \end{aligned}$$

The above equations were also used to estimate the errors in (ξ_i, ζ_i).

Settles [17] used the distance ξ_i in analyzing the inception length although other definitions can be formulated, e.g., r_i, where

$$r_i \approx r_v + \xi_i,$$

r_v being the distance from the fin apex, O, to the virtual origin, V (Fig. 5). The measured lengths are customarily normalized by δ and denoted with overbars; thus,

$$\bar{\xi}_i = \xi_i/\delta, \qquad \bar{r}_i = r_i/\delta, \qquad \text{etc.}$$

In the present study, since Re and δ were fairly constant, the effects of δ or Re_δ could not be explored.

3 Discussion of Results

Fig. 6 is a plot of $\bar{\xi}_i$ against α. This figure shows that $\bar{\xi}_i$ decreases as α increases. Thus, for a given Mach number, the inception length decreases as the interaction strength increases. Fig. 6 also shows that, for a given α, $\bar{\xi}_i$ increases with Mach number.

Previous studies [1, 10, 14] have shown that α is not an appropriate scaling parameter for fin interactions, but have shown that the inviscid shock-wave location plays an important role in characterizing the interaction. Therefore, the next step is to plot $\bar{\xi}_i$ against β_o which, apparently, serves as a shock-strength parameter (Fig. 7). It can be seen that the inception length, to first order, scales with β_o, with a slight decrease in $\bar{\xi}_i$ as M_∞ increases at a constant β_o, i.e.,

$$\bar{\xi}_i \approx f(\beta_o). \qquad (8)$$

Further, this scaling is nonlinear. When $\beta_o > 35°$, $\bar{\xi}_i$ becomes asymptotically constant and "small," being an order of magnitude less than when $\beta_o < 25°$. Thus, there appear to be two regimes in the inception-length scaling depending on how strong the interaction is. First-order curvefits to the two regimes are:

$$\begin{aligned} \bar{\xi}_i &= -43 + 1680/\beta_o, \quad 20° \lesssim \beta_o \lesssim 35°; \\ &\approx 3, \qquad\qquad\qquad \beta_o \gtrsim 35°; \end{aligned}$$

where β_o is in degrees.

The inception length behavior for $\beta_o \lesssim 20°$ could not be explored in the present tests. However, in hypersonic flows, β_o can easily be smaller than those found in the present tests; e.g., at $M_\infty = 8$, for $\alpha = 5°$, $\beta_o \approx 11°$. Care must therefore be exercised in extrapolating the present results to hypersonic Mach numbers. It appears that in typical hypersonic shock boundary-layer interaction experiments, measurements are usually taken within the inception zone, thus possibly accounting for discrepancies between supersonic and hypersonic results in, e.g., detecting conical symmetry [21]. Also, the present results show that speculation that hypersonic interactions have small inception lengths [13] may be incorrect since the behavior of the inception length is primarily dependent on β_o and not on M_∞.

Fig. 7 shows that, for strong interactions characterized by large β_o, there is almost no inception length. In other words, the interaction can be considered to be "fully developed" right from the apex. This has been observed by Zubin and Ostapenko [22] and is also evident in Law's results [23]. A small inception zone due to a large β_o can occur at low supersonic Mach numbers as well. However, data are generally unavailable for such an extreme circumstance, since stall in the test section prevents testing at large α to generate large-β_o shocks at, say, $M_\infty = 2$.

Further, the present result appears to be physically more realistic than those proposed in Eqs. (4), (5) and (6) which were based on a more limited dataset. In addition, the behavior of $\bar{\xi}_i$ with $\cot\beta_o$ for the present dataset is illustrated in Fig. 8. The good correlation between $\bar{\xi}_i$ and $\cot\beta_o$ can be expected if $\bar{\xi}_i$ scales with β_o because, in the range $20° \leq \beta_o \leq 40°$,

$$\cot\beta_o \sim 1/\beta_o.$$

For comparison with data reported by Settles [17], the present $M_\infty = 2.95$ data are normalized according to Eq. (3) and plotted in Fig. 9. This figure shows that the present estimate of $\bar{\xi}_i$ is typically two to three times less than the estimate of Settles [17] (Eq. (4)), with the disagreement becoming worse as $\cot\beta_o$ becomes small. The discrepancy is largely due to different methods in defining the inception length. In Ref. [17], the actual upstream-influence line was fitted with a line using a Kueffel & Esser No. 57168548 french curve. The inception point was then located as the intersection between the fitted line and a line parallel to the upstream-influence asymptote and 1 mm inboard. A crosscheck using the same french curve showed that, within 5% of ξ_i, estimates of ξ_i are the same between the present results and those of Ref. [17]. It is felt that the present method of extracting ξ_i data described previously is more accurate since there is no reason for the upstream-influence line to be constrained along a prescribed curve. In fact, since the inception and far-field conical regions of the interaction merge gradually, no *precise* definition of inception length is called for. Thus, the present work and Ref. [17] are not actually in conflict, even though the present criterion yields much shorter inception lengths. The key issue is thus not the criterion itself, as long as it is applied consistently to the entire dataset, but the trend of the inception length with Mach number and shock strength.

3.1 Physical Interpretation

The trend of the data, as depicted in Fig. 7, can be understood in terms of the relative importance of the inviscid and viscous parameters governing the interaction. As stated previously, δ and Re are held constant in this set of experiments so that their effects cannot be explored. A few general observations can, however, be made. It has often been observed that the interaction is predominantly inviscid [1, 13]. There appear to be two limits to the balance between viscous and inviscid parameters at, say, a given M_∞. The first occurs when an infinitesimally weak, swept shock wave impinges the boundary layer. This small, semi-infinite, inviscid disturbance sweeping across the boundary layer, arguably, should result in an infinitely-large $\bar{\xi}_i$ since the viscous effects outweigh the inviscid ones. (This would also give the appearance of cylindrical symmetry [14].) On the other hand, for large shock strengths, the inviscid parameters outweigh the viscous ones in determining the interaction behavior. Thus, as can be seen from the data, as the shock strength increases, ξ_i decreases until a "strong interaction" with a large β_o is developed. In such a circumstance, the incoming boundary layer imposes an apparently fixed, minimum (almost negligible) inception-length scale on the interaction. (A further exploration of the influence of δ and Re at the strong interaction limit would require larger values of δ and a broad range of Re.)

3.2 The Virtual Origin

For completeness, the nondimensional distance between the fin apex and the virtual origin, $\bar{r}_v$, is plotted against β_o in Fig. 10. The data scatter tends to be large [24, 25] because $\bar{r}_v$ is located by the intersection of two lines separated by a small angle. As also observed in Ref. [24], $\bar{r}_v$ decreases with increasing interaction strength. The present $\bar{r}_v$ data show a weak Mach number dependence when plotted against β_o, similar to the $\bar{\xi}_i$ behavior.

3.3 Final Remarks

The varying size of the inception length (Fig. 7) or, equivalently, the distance from the apex to the virtual origin (Fig. 10), has been a confusing factor in determining whether swept interactions are cylindrical or conical, as discussed in the Introduction. This can be further shown geometrically as follows. Referring to

Fig. 2, data in (x, z) coordinates can be transformed to (r, β) coordinates according to

$$r = \sqrt{(x - x_v)^2 + (z - z_v)^2}$$
$$\beta = \arctan[(z - z_v)/(x - x_v)].$$

It can be noted here that

$$\beta = \left(\theta + \frac{r_v}{s}\beta_o\right) \Big/ \left(1 + \frac{r_v}{s}\right), \qquad (9)$$

where (s, θ) constitute a polar-coordinate system centered at the fin apex. For simplicity, consider a point on the upstream-influence line (x_U, z_U). From Eq. (9), the difference between the angles β_U and θ_U can be expressed as

$$\beta_U - \theta_U = \frac{r_v/s}{1 + r_v/s}(\beta_o - \theta_U)$$

The above equation is displayed in Fig. 11. If $r_v = 0$, then

$$\beta_U = \theta_U.$$

For this limiting case, it cannot be conceived that $\beta_U = \beta_o$ unless $\beta_U \equiv \beta_o$, a physically impossible result since the (semi-infinite) interaction has to emanate from an origin. In other words, swept interactions without an inception zone *must* be conical. As a corollary, *all* swept interactions that show farfield cylindrical symmetry must have an inception zone.

In the other limit, when $r_v \to \infty$,

$$\beta_U = \beta_o.$$

This can be interpreted as follows. Weak interactions (which have large r_v) will appear cylindrical. Therefore, the cylindrical approximation for weak interactions can be accepted as valid. Finally, Fig. 11 shows that, for the range $0 \leq r_v < \infty$, the interaction is generally conical except that, for small values of $|\beta_o - \theta_U|$, say less than 2°, it is extremely difficult to distinguish if the interaction is cylindrical or conical.

The behavior of the interaction as described in the preceding paragraphs is deduced from a purely geometrical argument without considering whether the surface features are in the inception zone or in the farfield. This discussion serves to highlight the danger of misinterpreting the inception-zone data as exhibiting cylindrical symmetry. Data scatter in the farfield for weak interactions has been attributed in Ref. [14] as adding to this confusion. Fig. 11 shows that, for weak interactions where $|\beta_o - \theta_U|$ is small, such confusion can also arise in the inception zone.

4 Conclusions

The inception length to conical symmetry for fin-generated shock boundary-layer interactions was found to be weakly dependent on Mach number and to scale with the inviscid shock angle for $2.5 \leq M_\infty \leq 4$ and $4° \leq \alpha \leq 22°$. The inception length was found to be constant and small for strong interactions with shock angles larger than about 35°. Otherwise, the inception length was found to increase with decreasing shock angle. Physically, this inception-length behavior is attributed to the relative dominance of inviscid parameters over viscous parameters at large shock strengths.

Acknowledgements

The work reported in this paper was done by the first author during his Ph.D. research at the Gas Dynamics Laboratory, Penn State University. It was supported by AFOSR Grant 86-0082 from the U. S. Air Force Office of Scientific Research, monitored by Dr. L. Sakell, and by Joint Research Interchange NCA2-192 with the NASA Ames Research Center in which Dr. C. C. Horstman was the research collaborator.

References

[1] Settles, G. S. and Dolling, D. S., "Swept Shock Wave/Boundary-Layer Interactions," in *AIAA Prog. in Astronautics and Aeronautics: Tactical Missile Aerodynamics*, edited by M. Hemsch and J. Nielsen, Vol. 104, AIAA, Washington, D.C., 1986, pp. 297-379.

[2] Lu, F. K., "Fin Generated Shock-Wave Boundary-Layer Interactions," Ph.D. Thesis, The Pennsylvania State University, 1988.

[3] Settles, G. S. and Teng, H.-Y., "Flow Visualization Methods for Separated Three-Dimensional Shock Wave/Turbulent Boundary Layer Interactions," *AIAA J.*, Vol. 21, Mar. 1983, pp. 390-397.

[4] Lu, F. K. and Settles, G. S., "Color Surface-Flow Visualization of Fin-Generated Shock-Wave Boundary-Layer Interactions," accepted for publication in *Exp. Fluids*, 1989.

[5] Tobak, M. and Peake, D. J., "Topology of Three-Dimensional Separated Flows," *Ann. Rev. Fluid Mech.*, Vol. 14, 1982, pp. 61-85.

[6] Lu, F. K. and Settles, G. S., "Structure of Fin-Generated Shock-Wave Boundary-Layer Interactions by Laser Light-Screen Visualization," submitted to *J. Fluid Mech.*, 1988.

[7] Horstman, C. C., "Computation of Sharp-Fin-Induced Shock Wave/Turbulent Boundary-Layer Interactions," *AIAA J.*, Vol. 24, Sep. 1986, pp. 1433-1440.

[8] Horstman, C. C., "Prediction of Secondary Separation in Shock Wave Boundary-Layer Interactions," submitted to *Computers and Fluids*, 1988.

[9] Settles, G. S. and Teng, H.-Y., "Cylindrical and Conical Flow Regimes of Three-Dimensional Shock/Boundary-Layer Interactions," *AIAA J.*, Vol. 22, Feb. 1985, pp. 194-200.

[10] Settles, G. S. and Lu, F. K., "Conical Similarity of Shock/Boundary-Layer Interactions Generated by Swept and Unswept Fins," *AIAA J.*, Vol. 23, Jul. 1985, pp. 1021-1027.

[11] Wang, S.-Y. and Bogdonoff, S. M., "A Re-Examination of the Upstream Influence Scaling and Similarity Laws for 3-D Shock Wave/Turbulent Boundary-Layer Interaction," AIAA Paper 86-0347, Jan. 1986.

[12] Bogdonoff, S. M. and Wang, S.-Y., "Comment on 'Conical Similarity of Shock/Boundary-Layer Interactions Generated by Swept and Unswept Fins'," *AIAA J.*, Vol. 24, Mar. 1986, p. 540.

[13] Inger, G. R., "Spanwise Propagation of Upstream Influence in Conical Swept Shock/Boundary Layer Interactions," *AIAA J.*, Vol. 25, Feb. 1987, pp. 287-293.

[14] Lu, F. K., Settles, G. S. and Horstman, C. C., "Mach Number Effects on Conical Surface Features of Swept Shock Boundary-Layer Interactions," to be published in *AIAA J.*, 1989.

[15] Dolling, D. S. and Bogdonoff, S. M., "Upstream Influence in Sharp Fin-Induced Shock Wave Turbulent Boundary-Layer Interaction," *AIAA J.*, Vol. 21, Jan. 1983, pp. 143-145.

[16] Settles, G. S. and Bogdonoff, S. M., "Scaling of Two- and Three-Dimensional Shock/Turbulent Boundary-Layer Interactions at Compression Corners," *AIAA J.*, Vol. 20, June 1982, pp. 782-789.

[17] Settles, G. S., "On the Inception Lengths of Swept Shock-Wave/Turbulent Boundary-Layer Interactions," *Proc. of the IUTAM Symp. on Turbulent Shear-Layer/Shock-Wave Interactions*, edited by J. Délery, Palaiseau, France, Sept. 1985, Springer-Verlag, Berlin, 1986, pp. 203-213.

[18] McClure, W. B., "An Experimental Study into the Scaling of the Interaction of an Unswept Sharp Fin-Generated Shock/Turbulent Boundary Layer Interaction," M.S.E. Thesis, Princeton University, 1983.

[19] Sun, C. C. and Childs, M. E., "A Modified Wall-Wake Velocity Profile for Turbulent Compressible Boundary Layers," *AIAA J. of Aircraft*, Vol. 10, June 1973, pp. 318-383.

[20] Stalker, R. J., "Viscous Effects in Supersonic Flow," Ph.D. Thesis, University of Sydney, 1959.

[21] Holden, M. S., "Experimental Studies of Quasi-Two-Dimensional and Three-Dimensional Viscous Interaction Regions Induced by Skewed-Shock and Swept-Shock Boundary Layer Interaction," AIAA Paper 84-1677, June 1984.

[22] Zubin, M. A. and Ostapenko, N. A., "Structure of Flow in the Separation Region Resulting from Interaction of a Normal Shock Wave with a Boundary Layer in a Corner," *Izv. Akad. Nauk SSSR, Mekh. Zhid. i Gaza*, Vol. 14, May-June 1979, pp. 51-58, (Engl. trans.).

[23] Law, C. H., "Three-Dimensional Shock Wave-Turbulent Boundary Layer Interactions at Mach 6," ARL-TR-75-0191, June 1975.

[24] Lu, F. K., "An Experimental Study of Three-Dimensional Shock Wave Boundary Layer Interactions Generated by Sharp Fins," M.S.E. Thesis, Princeton University, 1983.

[25] Kimmel, R. L., "An Experimental Investigation of Quasi-Conical Shock wave/Turbulent Boundary Layer Interactions," Ph.D. Thesis, Princeton University, 1987.

Table 1 - Incoming freestream conditions

M_∞	p_o, MPa (psia)	T_o, K (°R)	$Re.10^{-6}$, m^{-1} (/ft)
2.47	$0.54 \pm 2.0\%$ (78)	$295 \pm 0.9\%$ (531)	$53.8 \pm 0.9\%$ (16.3)
2.95	$0.76 \pm 2.7\%$ (110)	$295 \pm 0.9\%$ (531)	$58.9 \pm 1.9\%$ (17.8)
3.44	$1.03 \pm 3.0\%$ (150)	$295 \pm 0.8\%$ (531)	$64.0 \pm 1.7\%$ (19.4)
3.95	$1.58 \pm 5.0\%$ (230)	$295 \pm 1.3\%$ (531)	$75.8 \pm 1.7\%$ (23.0)

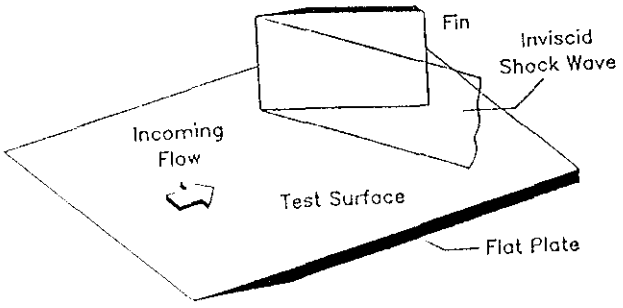

Figure 1: Fin.

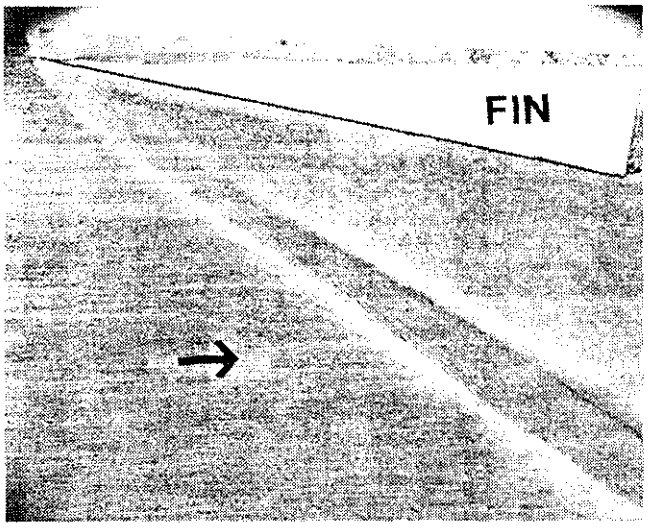

a. Example: $M_\infty = 2.95$, $\alpha = 15°$.

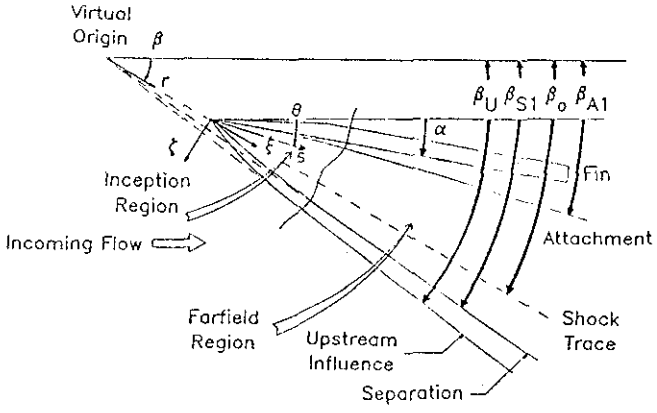

b. Sketch showing key surface features.

Figure 2: Surface-flow pattern in a fin-generated interaction.

Table 2 - Boundary layer parameters 216 mm (8.5 in) from the flat-plate leading edge

M_∞	δ, mm	θ, mm	$c_f.10^3$	Π
2.47	3.4 ± 0.1	0.21 ± 0.03	1.76 ± 0.03	0.56 ± 0.07
2.95	3.2 ± 0.1	0.18 ± 0.05	1.62 ± 0.08	0.72 ± 0.11
3.44	3.3 ± 0.1	0.16 ± 0.05	1.54 ± 0.10	0.54 ± 0.09
3.95	3.2 ± 0.1	0.13 ± 0.03	1.41 ± 0.11	0.58 ± 0.10

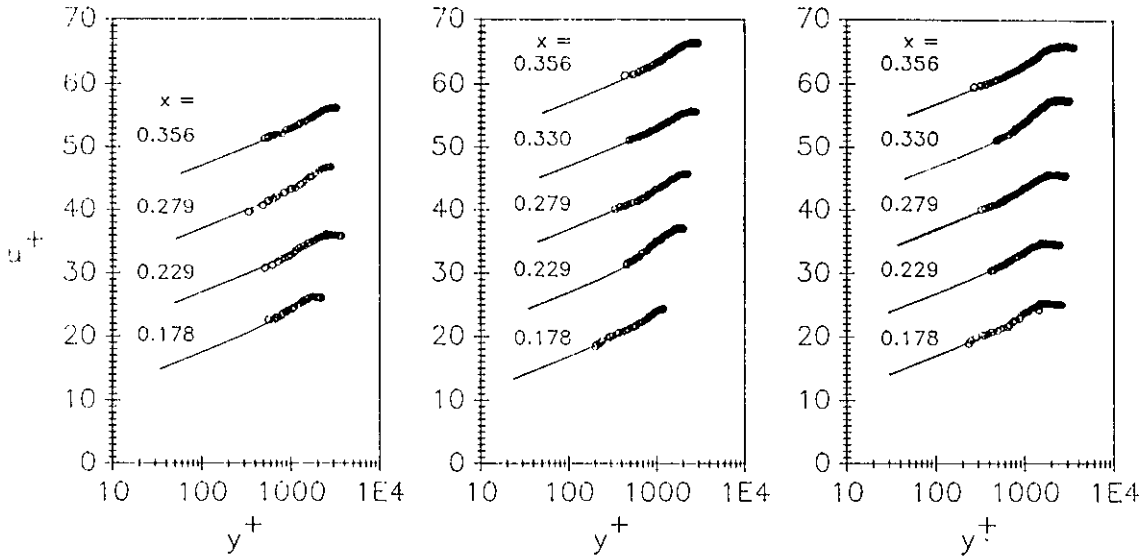

a. $M_\infty = 2.47$. b. $M_\infty = 2.95$. c. $M_\infty = 3.44$.

Figure 3: Undisturbed boundary-layer velocity profiles in wall coordinates.

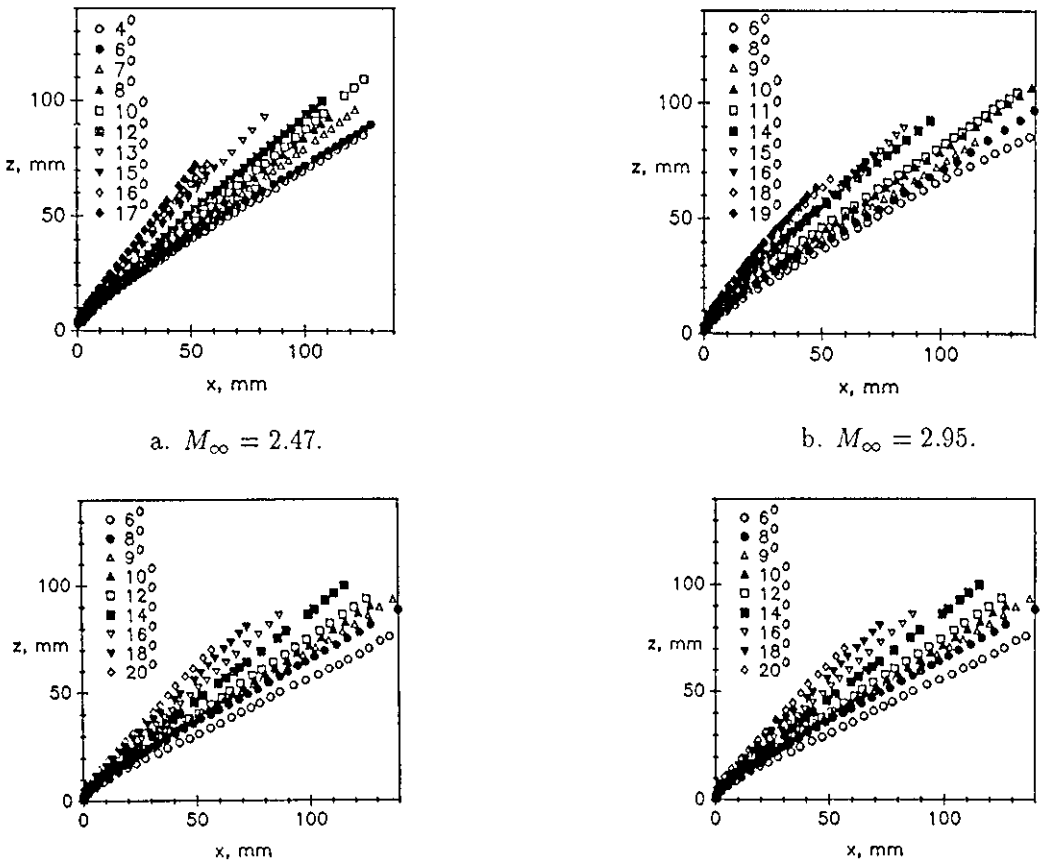

a. $M_\infty = 2.47$. b. $M_\infty = 2.95$.

c. $M_\infty = 3.44$. d. $M_\infty = 3.95$.

Figure 4: Upstream-influence lines.

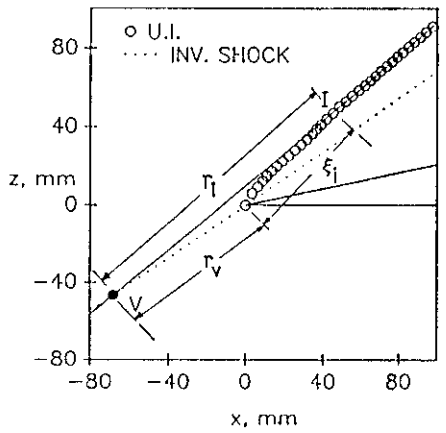

Figure 5: Example: $M_\infty = 2.47$, $\alpha = 12°$.

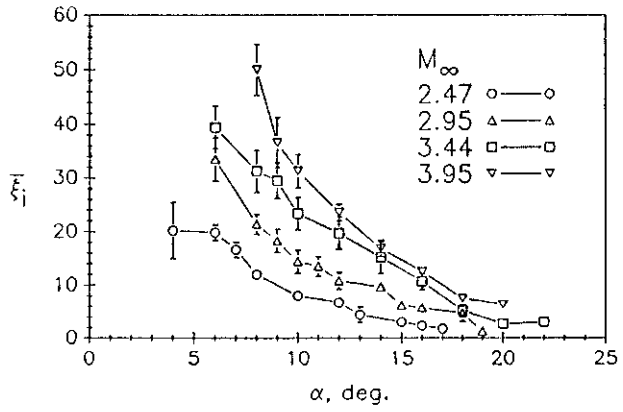

Figure 6: The trend of the inception length with fin angle.

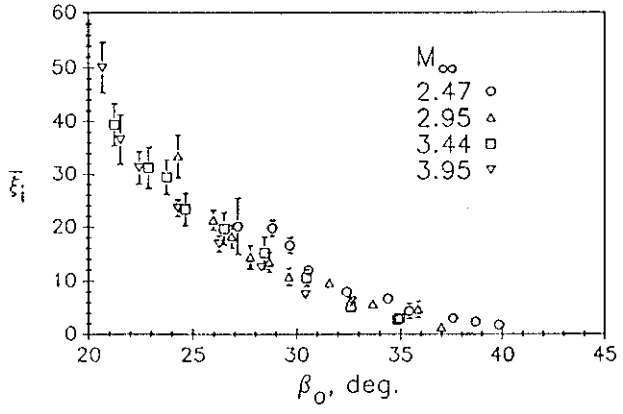

Figure 7: Scaling of the inception length with shock angle.

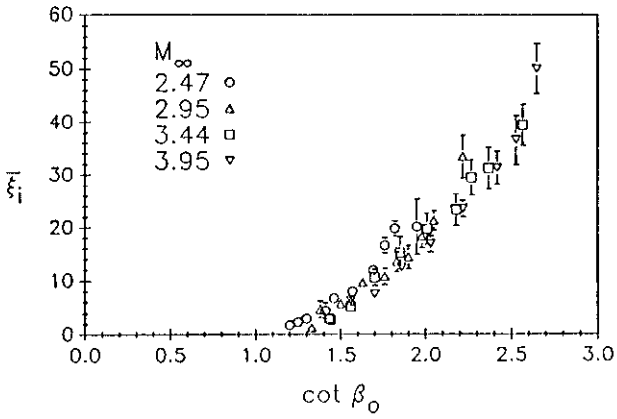

Figure 8: Scaling of the inception length with $\cot\beta_o$.

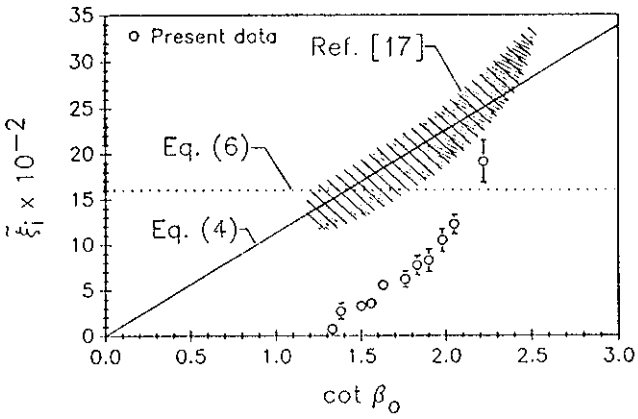

Figure 9: Scaling of $\tilde{\xi}_i$ with $\cot\beta_o$.

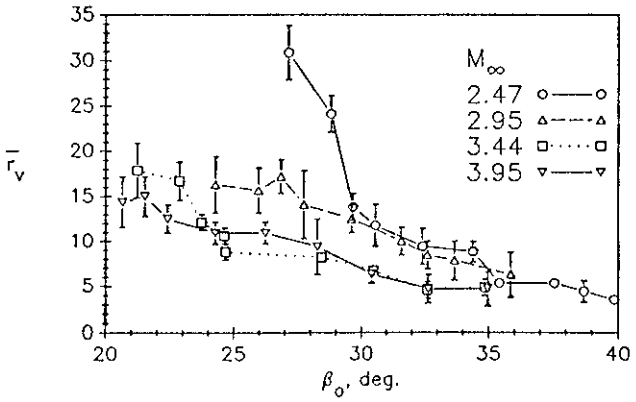

Figure 10: The virtual origin from the fin apex.

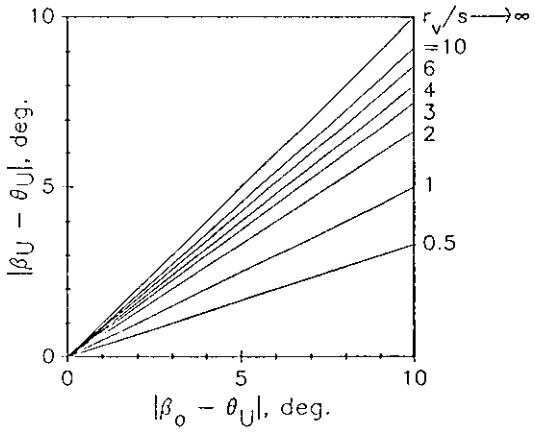

Figure 11: Cylindrical and conical symmetry by geometric considerations.